

Estimation of the thermal properties of an historic building wall by combining Modal Identification Method and Optimal Experiment Design

Julien Berger^{a*}, Benjamin Kadoch^b

November 18, 2021

^a Laboratoire des Sciences de l'Ingénieur pour l'Environnement (LaSIE), UMR 7356 CNRS, La Rochelle Université, CNRS, 17000, La Rochelle, France

^b Aix Marseille Université, CNRS, IUSTI UMR 7343, 13453 Marseille, France

*corresponding author, e-mail address : julien.berger@univ-lr.fr

Abstract

The estimation of wall thermal properties by *in situ* measurement enables to increase the reliability of the model predictions for building energy efficiency. Nevertheless, retrieving the unknown parameters has an important computational cost. Indeed, several computations of the heat transfer problem are required to identify these thermal properties. To handle this drawback, an innovative approach is investigated. The first step is to search the optimal experiment design among the sequence of observation of several months. A reduced sequence of observations of three days is identified which guarantees to estimate the parameter with the maximum accuracy. Moreover, the inverse problem is only solved for this short sequence. To decrease further the computational efforts, a reduced order model based on the modal identification method is employed. This *a posteriori* model reduction method approximates the solution with a lower degree of freedom. The whole methodology is illustrated to estimate the thermal diffusivity of an historical building that has been monitored with temperature sensors for several months. The computational efforts is cut by five. The estimated parameter improves the reliability of the predictions of the wall thermal efficiency.

Key words: Parameter estimation problem; Model Calibration; Inverse Heat Conduction Problem; Modal Identification Method; Reduced Order Model

1 Introduction

Within the environmental context, requirements on building energy efficiency becomes more and more important. In France, the building stock increases slowly [1] with an average around 1%. Thus, there is a crucial issue in retrofitting existing building. To this end, models such as building simulation programs are employed to define the best actions. However, there are some uncertainties on the input parameters of the model [2, 3]. Particularly, for such old buildings, the material properties may differ strongly from one site to another [4]. Indeed, due to the vernacular traditional architecture, the material were generally taken from locals around the building. Furthermore, the aging of materials may have changed the properties [5]. Parameter such as the thermal properties of the walls require to be known precisely since they play a crucial role on the assessment of the building energy efficiency [6, 7].

The unknown properties can be estimated by solving inverse problems or more precisely parameter estimation problem [8] to calibrate the model. This procedure aims at minimizing a so-called cost function between the model numerical predictions and the experimental observations obtained by on-site measurements. Such approaches have been successfully applied for real walls and a detailed state-of-the-art is proposed in [9]. However, the determination of thermo-physical properties using *in situ* dynamic measurements faces important challenge in terms of computational effort. This challenge arises from two reasons. The first one is the duration of the experimental observations. If long measurement duration are better for the accuracy of the retrieved parameter, it implies important computational costs to solve the inverse

problem. Note that *in situ* measurement depends also on occupants' acceptance and long period can be constraining. The standard techniques ISO 9869 requires more than a month of measurement periods [10]. Thus, various alternative techniques have been developed to reduced the monitoring time. In [11] an experiment of 7 days is carried. In [12], the accuracy of the parameter estimation is investigated according to the measurement period. For their case study, the authors suggest to carry at least three days of monitoring to have an accurate estimation. In [9], a fast estimation method is proposed based excitation pulse method and less than 1 h of measurement.

The second reason is the mathematical model to represent the physical phenomena. Indeed, the computational efforts required to solve the inverse problem are directly proportional to the so-called direct model (as well as the optimization algorithm). Thus, numbers of investigations aimed at developing direct model with reduced computational cost. Lumped model such as RC approaches have been proposed due to their very small computational cost. However, their reliability to estimate accurately the thermal diffusivity is questioned in [13]. The model has to be based on detailed heat diffusion process. In [14] an equivalent homogeneous model is proposed for the description of multi-layer walls with the issue of reducing the cost of parameter estimation as shown in [5]. When possible, analytical solution are also developed as for instance in [15].

Thus, the objective of this article is to answer both issues in order to propose a fast and accurate parameter estimation method. First, the length of the measurement observations is determined with the optimal experiment design methodology [16, 17]. The optimal design is searched according to the conditions of the experiment. Carrying the measurement for the optimal experiment design ensure to estimate the unknown parameter with the highest accuracy. This approach has been used in [18, 19] to determine the optimal boundary conditions of laboratory experiments to retrieve material properties of heat and mass transfer. In [20], an optimal design is found to retrieve the thermal conductivity and volumetric heat capacity of a material using laboratory experiments. This approach can be extended for *in-situ* measurement to determine the optimum sequence of measurement observations.

Then, to decrease the computational effort of the direct numerical model, model reduction techniques can be employed. Several methods are reported in the literature to model the physical phenomena in building walls [21]. Among all, the Modal Identification Method (MIM) demonstrated successful applications for inverse problem. The primer works of GIRAULT, PETIT, and VIDECOQ introduced the MIM approach for direct simulations in [22, 23]. Then, it has been applied for the identification of boundary fluxes through sequential procedure in [24–26] or surface temperature as in [27]. To our best knowledge, it has never been employed for the estimation of thermal diffusivity in building walls under climatic varying conditions. The MIM ROM is employed since in the state-space representation of the MIM model, both the field and its sensitivity to the unknown parameter are computed with a reduced computational cost. It can be combined with a gradient-based algorithm to retrieve the thermal properties of the wall.

This article presents and evaluate the proposed methodology to estimate the thermal diffusivity of a wall monitored in an old building. First the mathematical model is described in Section 2. The MIM model reduction method is detailed in Section 3. Then, the search optimal experiment design combined with the solution of the parameter estimation problem is presented in Section 4. A brief synthesis of the whole methodology and the metrics to evaluate its efficiency are given in Section 5. Subsequently, a first case study is introduced to validate the MIM method for estimating the thermal diffusivity of a wall. Last, a real case study is investigated in Section 7.

2 Mathematical model

First, the mathematical model is presented. It is based on two equations. The first corresponds to the diffusion one occurring in the wall. In addition, the sensitivity equation is also described. It enables to compute the sensitivity coefficient which qualifies the sensitivity of the field of temperature relative to change in the unknown diffusivity. This is required in the algorithm to solve the inverse problem.

2.1 Physical formulation

The field of interest is the temperature T evolving in a building wall material according to a diffusion process. The space domain is defined by $x \in [0, L]$, where L is the length of the wall. The time domain is defined by $t \in \Omega_t$ with $\Omega_t \stackrel{\text{def}}{=} [0, t_f]$. The temperature is computed using the heat diffusion equation [28]:

$$\frac{\partial T}{\partial t} = \alpha \cdot \frac{\partial^2 T}{\partial x^2}, \quad (1)$$

where $\alpha \stackrel{\text{def}}{=} \frac{k}{c}$ is the heat diffusion, k is the heat conductivity and c is the volumetric heat capacity. At the interface between ambient air and the wall, DIRICHLET type boundary conditions are assumed. The temperature is prescribed by the one measured:

$$\begin{aligned} T &= T_{\infty,L}(t), & x &= 0, \\ T &= T_{\infty,R}(t), & x &= L, \end{aligned}$$

where T_{∞} are the temperatures measured by sensors and depending on time:

$$T_{\infty} : t \mapsto T_{\infty}(t).$$

At $t = 0$, the temperature in the material is known:

$$T = T_{\text{ini}}(x), \quad t = 0.$$

with T_{ini} a function of x corresponding to the initial field in the wall:

$$T_{\text{ini}} : x \mapsto T_{\text{ini}}(x).$$

The so-called observable field T_s is defined as follows:

$$T_s : (x_s, t) \mapsto T(x_s, t), \quad s \in \{1, \dots, N_s\},$$

where N_s is the number of points of interests. In our case, it corresponds to the sensor locations. Thus, the observable fields correspond to the temperature computed with the model at the sensor locations. It enables to compare the model predictions with the experimental observations. The direct problem is now transformed into a dimensionless formulation to be solved by the numerical model.

2.2 Dimensionless formulation

As discussed and thoroughly motivated in [29, 30], it is of capital importance to obtain a dimensionless problem before elaborating a numerical model. It allows to define scaling parameters such as FOURIER number that may decrease the number of unknown parameters in the inverse problem. For this, dimensionless fields are defined:

$$\begin{aligned} u &\stackrel{\text{def}}{=} \frac{T - T_{\min}}{T_{\text{ref}}}, & u_{\infty,L} &\stackrel{\text{def}}{=} \frac{T_{\infty,L} - T_{\min}}{T_{\text{ref}}}, \\ u_{\infty,R} &\stackrel{\text{def}}{=} \frac{T_{\infty,R} - T_{\min}}{T_{\text{ref}}}, & u_{\text{ini}} &\stackrel{\text{def}}{=} \frac{T_{\text{ini}} - T_{\min}}{T_{\text{ref}}}, \end{aligned}$$

where T_{ref} and T_{\min} are user-defined reference temperature. The space and time coordinates are also transformed into dimensionless variables:

$$\begin{aligned} t^{\star} &\stackrel{\text{def}}{=} \frac{t}{t_{\text{ref}}}, & x^{\star} &\stackrel{\text{def}}{=} \frac{x}{L}. \end{aligned}$$

The FOURIER dimensionless number is defined:

$$\text{Fo} \stackrel{\text{def}}{=} \frac{t_{\text{ref}} \cdot \alpha}{L^2}.$$

It corresponds to the thermal diffusivity in the dimensionless representation and quantifies the magnitude of diffusion inside the material. A high number indicates a fast heat transfer process inside the material. With these transformations, the dimensionless problem is written as:

$$\frac{\partial u}{\partial t^*} = \text{Fo} \cdot \frac{\partial^2 u}{\partial x^{*2}} \quad (2)$$

with the boundary condition:

$$u = u_{\infty,L}(t), \quad x^* = 0 \quad (3a)$$

$$u = u_{\infty,R}(t), \quad x^* = 1 \quad (3b)$$

and the initial condition:

$$u = u_{\text{ini}}(x), \quad t^* = 0. \quad (4)$$

To have a well-posed problem, initial and boundary conditions must be compatible. The observable field is also transformed according to $u_s \stackrel{\text{def}}{=} \frac{T_s - T_{\text{min}}}{T_{\text{ref}}}$, $s \in \{1, \dots, N_s\}$.

2.3 Sensitivity equation

The issue is to estimate the unknown thermal diffusivity α of the wall or its equivalent in the dimensionless representation, the FOURIER number Fo . The solution of the inverse problem requires the so-called sensitivity function θ :

$$\theta : (\text{Fo}, x, t) \mapsto \frac{\partial u}{\partial \text{Fo}}.$$

It quantifies the sensitivity of the field of temperature according to the unknown parameter. A small magnitude reveals that large change in the parameter induces small change in the field. Thus, the parameter cannot be estimated with accuracy. Inversely, high magnitude of sensitivity coefficient are favorable conditions to estimate the unknown parameter. One can obtain can compute the sensitivity equations by differentiating Eq. (2) relatively to the parameter:

$$\frac{\partial \theta}{\partial t^*} = \text{Fo} \cdot \frac{\partial^2 \theta}{\partial x^{*2}} + \frac{\partial^2 u}{\partial x^{*2}}, \quad (5)$$

with the following boundary conditions obtained by differentiating Eq. (3):

$$\theta = 0, \quad x^* = 0,$$

$$\theta = 0, \quad x^* = 1,$$

and the initial condition arising from Eq. (4):

$$\theta = 0, \quad t^* = 0.$$

Particularly, the sensitivity function at the location x_s of the sensors are needed. It is computed by:

$$\theta_s : (x_s, t) \mapsto \theta(x_s, t), \quad s \in \{1, \dots, N_s\}.$$

3 MIM reduced order model of the field and its sensitivity

In this Section, the numerical models used to perform simulations are described starting first with the large original model. Then the reduced MIM approach is detailed. A uniform discretisation based on finite differences, is adopted for the space domain, with the discretisation parameter denoted by Δx . The discrete value of $u(x, t)$ and $\theta(x, t)$ becomes $u_j \stackrel{\text{def}}{=} u(x_j, t)$ and $\theta_j \stackrel{\text{def}}{=} \theta(x_j, t)$, respectively, with $j \in \{1, \dots, N\}$. Note that other discretisation methods (finite volumes, finite elements, ...) could be used and will give the same MIM formulation.

3.1 The state space representation of the large original model

The straightforward semi-discretization of Eqs. (2) and (5) using central finite differences yields for $j \in \{2, \dots, N-1\}$ to:

$$\frac{\partial u}{\partial t} = \frac{\text{Fo}}{\Delta x^2} \cdot (u_{j+1} - 2 \cdot u_j + u_{j-1}), \quad (6a)$$

$$\frac{\partial \theta}{\partial t} = \frac{\text{Fo}}{\Delta x^2} \cdot (\theta_{j+1} - 2 \cdot \theta_j + \theta_{j-1}) + \frac{1}{\Delta x^2} \cdot (u_{j+1} - 2 \cdot u_j + u_{j-1}). \quad (6b)$$

The problem is governed by DIRICHLET boundary conditions for both fields u and θ :

$$u_1 = u_{\infty, L}(t), \quad u_N = u_{\infty, R}(t), \quad \theta_1 = 0, \quad \theta_N = 0.$$

Thus, the semi-discrete equations (6) can be written in the matrix form:

$$\begin{aligned} \dot{\mathbf{U}} &= \text{Fo} \cdot \mathbf{A} \cdot \mathbf{U} + \text{Fo} \cdot \mathbf{B} \cdot \mathbf{Q}, \\ \dot{\boldsymbol{\Theta}} &= \text{Fo} \cdot \mathbf{A} \cdot \boldsymbol{\Theta} + \mathbf{A} \cdot \mathbf{U} + \mathbf{B} \cdot \mathbf{Q}, \end{aligned}$$

where $\mathbf{A} \in \mathcal{M}(\mathbb{R}^{N \times N})$ and $\mathbf{B} \in \mathcal{M}(\mathbb{R}^{N \times 2})$ are matrices defined to ensure a second order accuracy in space:

$$\mathbf{A} \stackrel{\text{def}}{=} \frac{1}{\Delta x^2} \cdot \begin{bmatrix} -2 & 1 & 0 & \dots & 0 \\ 1 & -2 & 1 & \ddots & 0 \\ 0 & \ddots & \ddots & \ddots & 0 \\ 0 & \dots & 1 & -2 & 1 \\ 0 & \dots & 0 & 1 & -2 \end{bmatrix}, \quad \mathbf{B} \stackrel{\text{def}}{=} \begin{bmatrix} 1 & 0 \\ 0 & 0 \\ \vdots & \vdots \\ 0 & 0 \\ 0 & 1 \end{bmatrix}, \quad \mathbf{Q} \stackrel{\text{def}}{=} [u_{\infty, L} \quad u_{\infty, T}]^\top$$

The computation of the observable fields u_s and θ_s can also be formulated in a matrix form:

$$\mathbf{Y}_u = \mathbf{C} \cdot \mathbf{U}, \quad \mathbf{Y}_\theta = \mathbf{C} \cdot \boldsymbol{\Theta}.$$

where $\mathbf{C} \in \mathcal{M}(\mathbb{R}^{N_s \times N_s})$, so that $\mathbf{Y}_u \in \mathcal{M}(\mathbb{R}^{N_s \times 1})$ and $\mathbf{Y}_\theta \in \mathcal{M}(\mathbb{R}^{N_s \times 1})$ are vectors. In the end, the state space representation of the problem is formulated as:

$$\begin{cases} \dot{\mathbf{U}} &= \text{Fo} \cdot \mathbf{A} \cdot \mathbf{U} + \text{Fo} \cdot \mathbf{B} \cdot \mathbf{Q}, \\ \dot{\boldsymbol{\Theta}} &= \text{Fo} \cdot \mathbf{A} \cdot \boldsymbol{\Theta} + \mathbf{A} \cdot \mathbf{U} + \mathbf{B} \cdot \mathbf{Q}, \\ \mathbf{Y}_u &= \mathbf{C} \cdot \mathbf{U}, \\ \mathbf{Y}_\theta &= \mathbf{C} \cdot \boldsymbol{\Theta}. \end{cases} \quad (7)$$

The model is solved using a RUNGE-KUTTA order 2 solver. It computes the field and its sensitivity at the points of interests x_s , corresponding to the sensor locations. It is denoted as Large Original Model (LOM).

3.2 The MIM reduced order model

The MIM reduced order model enables to compute the field \tilde{u}_s and $\tilde{\theta}_s$, $s \in \{1, \dots, N_s\}$. They are gathered in the vectors $\tilde{\mathbf{Y}}_u$ and $\tilde{\mathbf{Y}}_\theta$. Both are computed from the unknown reduced vectors $\mathbf{X}_u \in \mathcal{M}(\mathbb{R}^{N_r \times 1})$ and $\mathbf{X}_\theta \in \mathcal{M}(\mathbb{R}^{N_r \times 1})$. The reduced model equations is assumed as:

$$\begin{cases} \dot{\mathbf{X}}_u &= \text{Fo} \cdot \mathbf{F} \cdot \mathbf{X}_u + \text{Fo} \cdot \mathbf{G} \cdot \mathbf{Q}, \\ \dot{\mathbf{X}}_\theta &= \text{Fo} \cdot \mathbf{F} \cdot \mathbf{X}_\theta + \mathbf{F} \cdot \mathbf{X}_u + \mathbf{G} \cdot \mathbf{Q}, \\ \tilde{\mathbf{Y}}_u &= \mathbf{H}_u \cdot \mathbf{X}_u, \\ \tilde{\mathbf{Y}}_\theta &= \mathbf{H}_\theta \cdot \mathbf{X}_\theta, \end{cases} \quad (8)$$

where the matrix $\mathbf{F} \in \mathcal{M}(\mathbb{R}^{N_r \times N_r})$ is assumed as diagonal. And the matrices $\mathbf{G} \in \mathcal{M}(\mathbb{R}^{N_r \times 2})$, $\mathbf{H}_u \in \mathcal{M}(\mathbb{R}^{N_s \times N_r})$ and $\mathbf{H}_\theta \in \mathcal{M}(\mathbb{R}^{N_s \times N_r})$ are full. Indeed the general formulation of MIM (Eq. 8) is obtained by considering the transformation $\mathbf{U} = \mathbf{M}\mathbf{X}_u$ applied to the LOM equations (Eq. 7). It can be noted that the columns of the matrix $\mathbf{M} \in \mathcal{M}(\mathbb{R}^{N \times N_r})$ contains the eigenvectors of \mathbf{A} and the diagonal matrix $\mathbf{F} \in \mathcal{M}(\mathbb{R}^{N_r \times N_r})$ the N_s eigenvalues of \mathbf{A} .

The reduced model will thus give at time t the reduced vectors \mathbf{X}_u and \mathbf{X}_θ . To come back to the fields at the interest points, the operations $\tilde{\mathbf{Y}}_u = \mathbf{H}_u \cdot \mathbf{X}_u$ and $\tilde{\mathbf{Y}}_\theta = \mathbf{H}_\theta \cdot \mathbf{X}_\theta$ are performed. These observable fields are obtained by the reduced model and thus denoted with the super script \sim . It is interesting to remark that knowing matrices \mathbf{F} , \mathbf{G} , we have straightforwardly the reduced model for the sensitivity \mathbf{X}_θ . Here, the MIM model is solved using a RUNGE–KUTTA order 2 method.

The construction of the MIM reduced model is performed by defining the differences between the reduced model and the complete model as a square residues functional J_{rom} :

$$J_{rom}(N_r, \mathbf{F}, \mathbf{G}, \mathbf{H}_u, \mathbf{H}_\theta) \stackrel{\text{def}}{=} \sum_{i=1}^{N_s} \int_0^{t_f} \left(\frac{\tilde{u}_s(t) - u_s(t)}{u_s(t)} \right)^2 + \left(\frac{\tilde{\theta}_s(t) - \theta_s(t)}{\theta_s(t)} \right)^2 dt.$$

The functional J_{rom} is minimized to determined the order of the reduced model N_r and matrices \mathbf{F} , \mathbf{G} , \mathbf{H}_u and \mathbf{H}_θ . The minimization procedure is carried out preliminary to the solution of the parameter estimation problem, using any optimizer such as quasi-Newton, PSO or genetic algorithm. This procedure is denoted as the *learning step*. Here the construction is performed for several values of the unknown diffusivity α . The set of thermal diffusivity used for the construction of the ROM is denoted Ω_α .

4 Parameter estimation problem with reduced order model

The reduced order model is used in the framework of parameter estimation problem. For the sake of clarity, the methodology is explained for the unknown parameter denoted by:

$$p = \alpha.$$

It is also distinguished the solution of the parameter estimation problem p° . It is different from the exact solution of the problem, noted p^r , when known. The so-called *a priori* parameter, used as initial guess in the algorithm to solve the inverse problem, is denoted by p^{apr} . The set of searched parameter is denoted Ω_p . The experimental observations of the field u are written with the super-script m . Thus, the vector of observation is denoted $\mathbf{Y}^m \in \mathcal{M}(\mathbb{R}^{N_s \times 1})$.

4.1 The optimal sequence of observations

To use the MIM ROM in the framework of parameter estimation problem, it requires a learning step to build *a posteriori* the matrices. Since this step is time consuming, the optimal experiment design (OED) methodology [19, 31] is used to select a reduced measurement sequence of 3 days, denoted:

$$\Omega_t^{\text{oed}} \stackrel{\text{def}}{=} [t_{\text{ini}}, t_{\text{ini}} + 3],$$

where $t_{\text{ini}} [\text{d}]$ is the beginning of the reduced sequence. Note that the reduced sequence respects the condition $\Omega_t^{\text{oed}} \subset \Omega_t$. The measurement plan Π is introduced:

$$\Pi = \{t_{\text{ini}}\},$$

The search of the optimal measurement plan Π° is carried out through the maximization of the D-criteria [16, 17]

$$\Pi^\circ = \arg \max_{\Pi} \Psi,$$

where Ψ is the determinant of the FISHER matrix \mathcal{F} :

$$\Psi \stackrel{\text{def}}{=} \det \mathcal{F}(\Pi),$$

and

$$\mathcal{F} \stackrel{\text{def}}{=} \frac{1}{\sigma^2} \sum_{i=1}^{N_s} \int_{\Omega_t^{\text{oed}}} \theta_s(t)^2 dt,$$

with σ is the measurement uncertainty. This methodology is performed using the LOM and the *a priori* value of the unknown parameter. It enables to determine the optimal reduced sequence of measurement that maximize the parameter estimation accuracy. With this approach, the learning step of the MIM and the solution of the inverse problem are performed over a reduced sequence $\Omega_t^{\text{oed}} \subset \Omega_t$.

4.2 Estimating the unknown parameter

The parameter estimation problem is solved over the reduced sequence Ω_t^{oed} to cut the computational efforts. It aims at determining the unknown parameter p verifying:

$$p^\star = \min_{\Omega_p} J(p),$$

where J is the cost function defined using the least square estimator and the reduced model:

$$J : p \mapsto \sum_{i=1}^{N_s} \int_0^{t_f} \left(\tilde{u}_s(p, t) - u_s^m(t) \right)^2 dt. \quad (9)$$

The minimisation of the cost function is realized using the GAUß algorithm [17, 28]. It assumes the following condition on J :

$$\nabla_p J = 0. \quad (10)$$

Thus, Eq. (10) is equivalent to:

$$\sum_{i=1}^{N_s} \int_0^{t_f} \tilde{\theta}_s(p, t) \cdot \left(\tilde{u}_s(p, t) - u_s^m(t) \right) = 0. \quad (11)$$

Using the TAYLOR expansion of \tilde{u} around a parameter p^k , equation (11) gives a system of N_s equations:

$$\left(\tilde{u}_s(p^k, t) + \tilde{\theta}_s(p^k, t) \cdot (p - p^k) - u_s^m \right) = \mathbf{0}.$$

It enables to compute the next candidate $p = p^{k+1}$ better than p^k in an iterative procedure, written with the matrix formulation:

$$p^{k+1} = p^k + \left(Y_\theta^\top(p^k) \cdot Y_\theta(p^k) \right)^{-1} \cdot Y_\theta(p^k) \cdot \left(Y^m - \tilde{Y}_u(p^k) \right). \quad (12)$$

In terms of computational time, the cost to compute the new candidate p^{k+1} is strongly reduced due to the use of MIM reduced order model. Indeed, it only manipulates the reduced vectors \mathbf{X}_u and \mathbf{X}_θ of size $N_r \ll N_s$. Moreover, the MIM model provides straightforwardly the sensitivity functions of the observable fields.

The Algorithm 1 describes the main steps to solve the inverse problem. At the iteration k , the field and its sensitivity are computed using the MIM ROM and a candidate p_k for the unknown parameter. With these results, the cost function between measurement and model predictions is evaluated. Moreover, using the sensitivity \mathbf{Y}_θ , the candidate p_{k+1} for the next iteration is computed. The algorithm runs until a maximum number of iterations N_k is reached or one of the two following criteria is satisfied:

$$\gamma_1 \geq \eta_1 \quad \& \quad \gamma_2 \geq \eta_2,$$

where η_1 and η_2 are user defined values. The criteria γ_1 and γ_2 evaluates the relative magnitude changes of the cost function and candidate parameter, respectively:

$$\gamma_1 \stackrel{\text{def}}{=} \frac{\|J(p_{k+1}) - J(p_k)\|_2}{\|J(p_k)\|_2}, \quad \gamma_2 \stackrel{\text{def}}{=} \frac{\|p_{k+1} - p_k\|_2}{\|p_k\|_2}.$$

Algorithm 1 GAUß algorithm using the MIM ROM.

- 1: Build matrices \mathbf{F} , \mathbf{G} , \mathbf{H}_u and \mathbf{H}_θ according to MIM learning step
 - 2: Set iteration indicator $k = 1$
 - 3: Set *a priori* parameter $p_k = p^{\text{apr}}$
 - 4: **while** $k \leq N_k$ & $\gamma_1 \geq \eta_1$ & $\gamma_2 \geq \eta_2$ **do**
 - 5: Compute the direct problem \mathbf{Y}_u and \mathbf{Y}_θ using reduced order model with Eq. (8) and a candidate p_k
 - 6: Evaluate the cost function J using Eq. (9)
 - 7: Compute the next candidate for the unknown parameter p_{k+1} using Eq. (12)
 - 8: Increment: $k = k + 1$, $p_k \leftarrow p_{k+1}$
 - 9: Compute stopping criteria γ_1 and γ_2 with Eqs.
 - 10: **end**
-

5 Synthesis of the methodology and metrics of its efficiency

The global methodology to solve the parameter estimation problem of heat transfer using MIM ROM is synthesized in Fig. 1. First, the OED methodology is used to define an optimal reduced sequence Ω_t^{OED} of the observations of the field. This results have two advantages noticeable at steps two and three. At step two, the learning step of the MIM is carried only for 3 days and not for the whole signal. It saves important computational efforts to determine the matrices of the ROM MIM. Then, at step three, the inverse problem is solved for a reduced sequence. Moreover, the sequence is optimal since it ensures the maximum accuracy of the retrieved parameters. Last, when the unknown parameter is estimated, the MIM

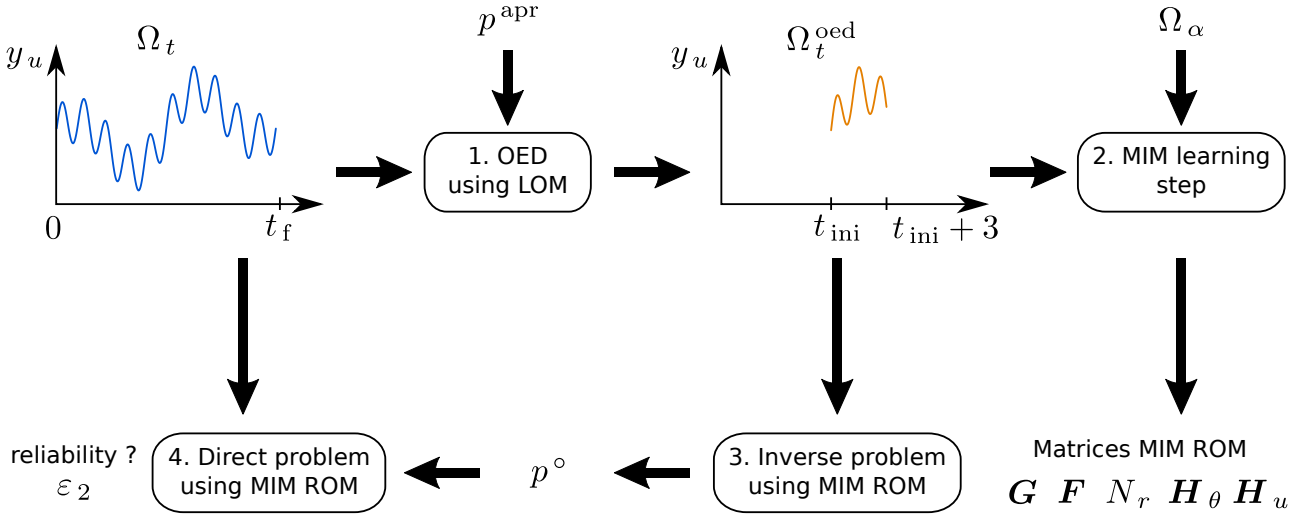


Figure 1. *illustration of the methodology.*

ROM is computed considering the whole signal. The error between the numerical predictions and the whole sequence of experimental observations is computed to evaluate the reliability of the model.

Several metrics are defined to evaluate the efficiency of the proposed method. The \mathcal{L}_2 and \mathcal{L}_∞ errors are denoted by ε_2 and ε_∞ , respectively. They are computed to evaluate the accuracy of the predictions of the numerical models:

$$\varepsilon_2 \stackrel{\text{def}}{=} \sqrt{\frac{1}{N_s N_t} \sum_{n=1}^{N_t} \sum_{s=1}^{N_s} \left(u(x_s, t_n) - u^{\text{ref}}(x_s, t_n) \right)^2},$$

$$\varepsilon_\infty \stackrel{\text{def}}{=} \max_{x_s, t_n} \left| u(x_s, t_n) - u^{\text{ref}}(x_s, t_n) \right|,$$

where u^{ref} is a so-called reference solution, obtained generally by the LOM model, and N_t the number of time step. In addition, the relative error ε_r is calculated to evaluate the accuracy of the retrieved parameter:

$$\varepsilon_r \stackrel{\text{def}}{=} \frac{p^\circ - p^r}{p^r}.$$

Another important criteria is the computational efforts evaluated in the **Matlab** environment with a computer equipped with **Intel i7** CPU and 32 GB of RAM. The measured computational time is denoted by $t_{\text{cpu}} [\text{s}]$. A dimensionless version is also computed:

$$t_{\text{cpu}}^* \stackrel{\text{def}}{=} \frac{t_{\text{cpu}}}{t_{\text{cpu}, \text{ref}}},$$

where $t_{\text{cpu}, \text{ref}}$ corresponds to the computational time required using the LOM.

6 Validation of the MIM model for parameter estimation problem

The construction of the MIM ROM and its use to solve parameter estimation problem is first explained on a simple case with simulated experimental data. Since the computational costs are reduced, step one of the methodology illustrated in Figure 1 is not carried out. Thus, next section presents the learning step to build the MIM ROM for the field and its sensitivity to the unknown parameter. Then, the model is used for parameter estimation problem.

6.1 Construction of the MIM ROM

The MIM ROM is built during the so-called learning step. For this, Eq. (1) is solved for a wall of length $L = 0.5$ m, an horizon of simulation $t_f = 24$ h and the following initial and right boundary condition:

$$T_{\text{ini}} = T_{\infty, R} = 20 \text{ }^{\circ}\text{C}.$$

The solution is generated for four cases at five points of interests defined as:

$$x_s = \{0.1, 0.15, 0.25, 0.3, 0.45\}. \quad (13)$$

Three cases corresponds to the following diffusivity $\Omega_{\alpha} = \{2.03, 5.21, 5.81\} \cdot 10^{-7} \text{ m}^2 \cdot \text{s}^{-1}$, corresponding to the ones of concrete, gypsum and mineral wool, combined with the left boundary condition:

$$T_{\infty, L}^1 = T_{\text{ini}} + 5 \sin\left(\frac{2\pi}{24 \cdot 3600} t\right). \quad (14)$$

The last case is carried out for the diffusivity of concrete $\alpha = 5.21 \cdot 10^{-7} \text{ m}^2 \cdot \text{s}^{-1}$ and a slightly modified left boundary condition:

$$T_{\infty, L}^2 = T_{\text{ini}} + 20 \sin\left(\frac{6\pi}{24 \cdot 3600} t\right). \quad (15)$$

To obtain each order of the MIM, PSO is used to perform the learning step with 100 iterations and a size of 50 populations. It can be noted that taking 100 iterations is more than sufficient to ensure the convergence.

Figures 2(a) and 2(b) show the error of the reduced order model with the order N . After the order 10, the accuracy of the model becomes stable. Thus, a MIM ROM with an order N scaling with $\mathcal{O}(5)$ enables to cut the computational complexity as well as ensure a sufficient accuracy of the predictions.

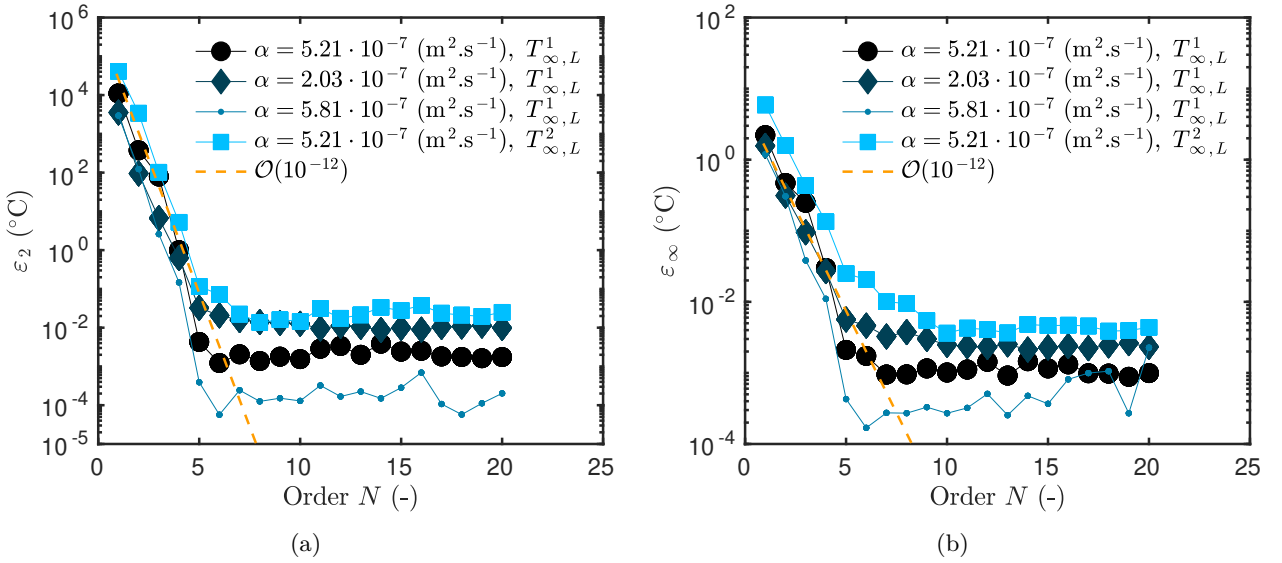


Figure 2. Evolution of the error of the MIM ROM model according to the order N .

6.2 Accuracy for direct simulations

To evaluate the accuracy of the built model, the solutions y_u and y_{θ} are computed with the MIM ROM and the LOM for 50 values of α in the interval $[2.03, 6.37] \cdot 10^{-7} \text{ m}^2 \cdot \text{s}^{-1}$. The following initial and boundary conditions are defined:

$$T_{\text{ini}} = T_{\infty, R} = 20 \text{ }^{\circ}\text{C}, \quad T_{\infty, L} = T_{\text{ini}} + 5 \sin\left(\frac{2\pi}{24 \cdot 3600} t\right).$$

Table 1. Efficiency of the MIM ROM.

Model	Order	ε_∞		$t_{\text{cpu}} [\text{s}]$		$t_{\text{cpu}}^* [-]$	
		u_s	θ_s	Learning step	Direct simulation	Learning step	Direct simulation
LOM	75	-	-	-	0.60	-	1
ROM	17	0.08	0.06	2.4	0.10	4	0.16
ROM	5	0.07	0.06	2.4	0.08	4	0.13

The final time is $t_f = 24 \text{ h}$ and the wall of length $L = 0.5 \text{ m}$. The points of interest are the same as defined in Eq. (13). The discretisation parameters is $\Delta t = 30 \text{ s}$ for both models. For the LOM, 75 points of space discretisation are used.

The time evolution of the fields and the sensitivity at the five points of interests is shown in Figures 3(a) and 3(b) for two values of diffusivity, obtained with the MIM order 5. It highlights that the model enables to simulate the whole dynamic of the observable outputs for thermal diffusivity different from the one used in the learning step.

Figure 4 shows the variation of the error according to the values of the diffusivity and for two different orders. The ROM of order 5 has a satisfactory error, lower than 10^{-1} for both the field and its sensitivity. Moreover, the error is stable for the whole range of thermal diffusivity remaining inside the domain used during the learning step. As noted for $\alpha > 6 \cdot 10^{-7} \text{ m}^2 \cdot \text{s}^{-1}$, the accuracy of the model is not satisfying anymore. Indeed, this diffusivity is out of the range used during the learning step.

Table 1 provides a synthesis of the efficiency of the MIM ROM for a direct simulation. The accuracy of the model is almost similar between order 5 and 17. In terms of computational time, the MIM ROM of order 5 enables to cut the computational cost by 87% compared to the LOM. Since the model reduction method is *a posteriori*, there is an inherent computational cost to build the MIM model. As a synthesis, a learning step composed of 4 signals is sufficient to build a model of low order and reliable for a wide range of parameter α .

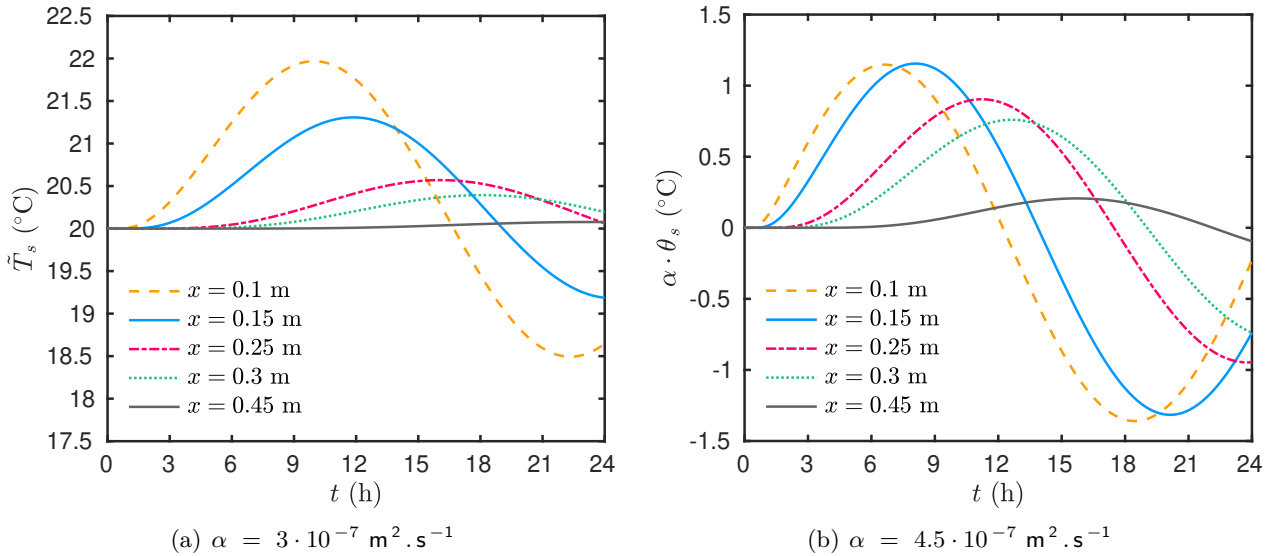


Figure 3. Evolution of the field and the sensitivity at the points of interest for two values of diffusivity.

6.3 Parameter estimation problem

The reliability of the MIM ROM is now evaluated for solving parameter estimation problem. For this, experimental observations are numerically generated using the LOM for a diffusivity $\alpha^r = 5.21 \cdot 10^{-7} \text{ m}^2 \cdot \text{s}^{-1}$.

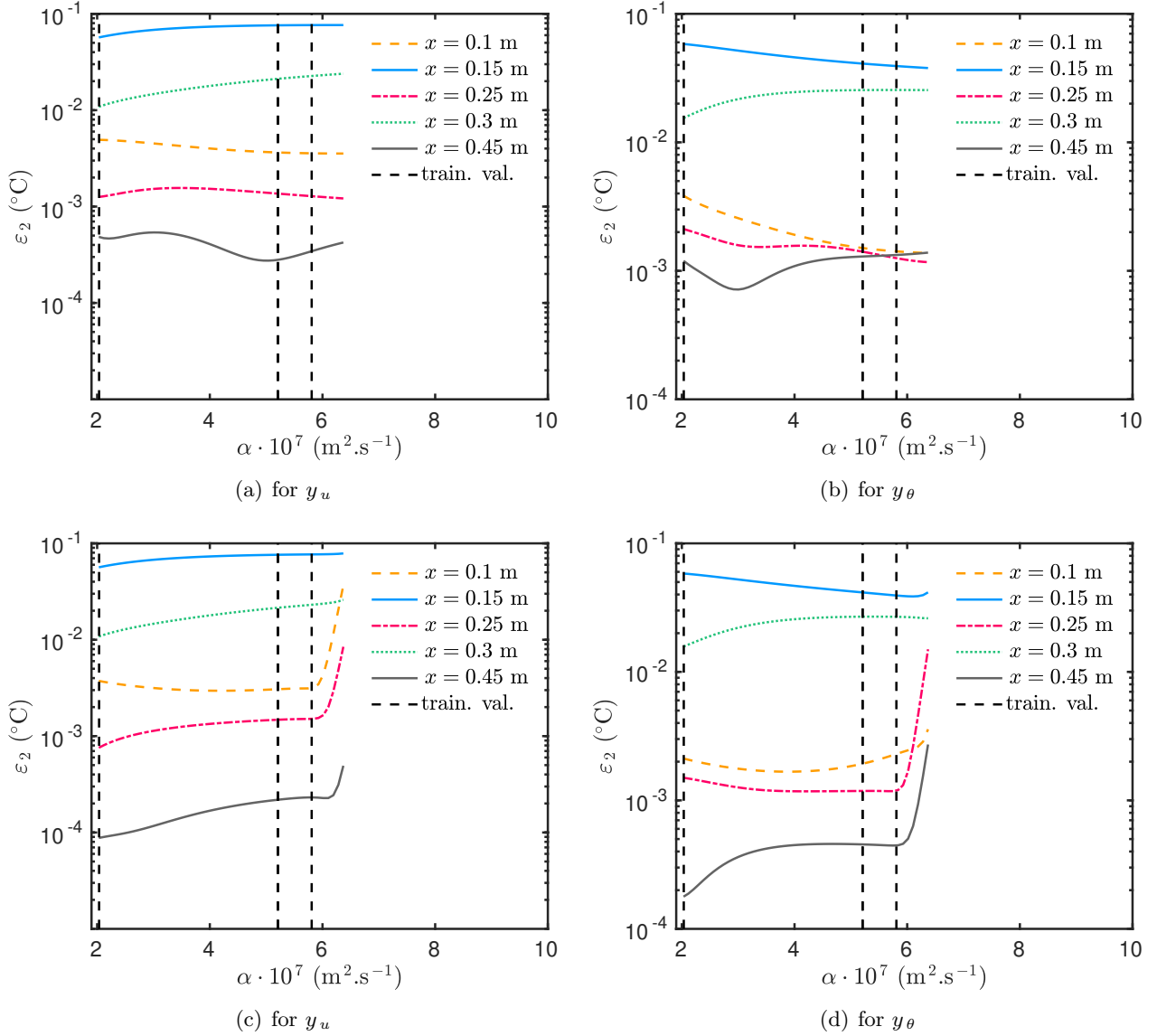


Figure 4. Variation of the error of the MIM ROM, Orders 5 (a,b) and 17 (c,d), for the whole interval of thermal diffusivity, for the field (a,c) and its sensitivity (b,d).

The initial and boundary conditions are the following:

$$T_{\text{ini}} = T_{\infty, R} = 20 \text{ }^\circ\text{C}, \quad T_{\infty, L} = T_{\text{ini}} + 3 \cdot \left(1 - \cos\left(\frac{2\pi}{12 \cdot 3600} t\right) \right).$$

It can be remarked that the boundary condition at $T_{\infty, L}$ is very different from the one used during the learning step of the MIM ROM (14) and (15). The LOM is computed using $\Delta t = 30 \text{ s}$ and $\Delta x = 6.8 \text{ mm}$. Then, the observations are projected at the points of interest considering a time step of 1 hour and adding a random normally distributed error. The standard deviation of the measurement is reported in Table 2.

Both the LOM and the MIM ROM of order 5 are used to solve the parameter estimation problem. The initial guess is $\alpha^{\text{apr}} = 2.1 \cdot 10^{-7} \text{ m}^2 \cdot \text{s}^{-1}$, corresponding to a different value from those used during the learning step. The stopping criteria are set as $\eta_1 = \eta_2 = 10^{-14}$ and $N_k = 100$. The convergence of the algorithm to solve the parameter estimation problem is illustrated in Figures 5(a) and 5(b). The algorithm searches the unknown parameter until the criteria γ_2 on the cost function is lower than 10^{-14} . It requires 8 and 10 iterations when using the LOM and the ROM, respectively. A comparison of the model prediction with the estimated parameters against the measurement is shown in Figures 6(a) and 6(b). A satisfying

Table 2. Results of the parameter estimation problem.

Model	Point of observation x_s [m]					Error ε_r [-] on				
	0.1	0.15	0.25	0.3	0.45	Computational time		parameter estimation		
	Error ε_2					Order	t_{cpu} [s]	t_{cpu}^* [-]	α^{apr}	α°
LOM	0.059	0.092	0.073	0.10	0.073	75	4	1	-0.59	-0.01
ROM	0.068	0.11	0.083	0.10	0.074	5	0.9	0.23	-0.59	-0.04
Measurement uncertainty [°C]										
	0.94	0.70	0.46	0.30	0.13					

accuracy is observed for both models. The residuals have no specific signature as illustrated in Figures 6(c) and 6(d). Table 2 provides a synthesis of the results. The MIM ROM enables to cut the computational time to solve the inverse problem with a satisfying relative error of 4% on the estimated parameter.

Further numerical tests are carried for 50 values of thermal diffusivity. Figure 7(a) shows the evolution of the estimated parameter using the MIM ROM of order 5. The algorithm requires around 5 iterations to estimate the unknown parameters with an relative accuracy of 4%. Figure 7(b) gives the variation of the computational time ratio between the algorithm using the LOM and the MIM ROM. The use of the reduced order model enables to reduce the computational effort by 60%.

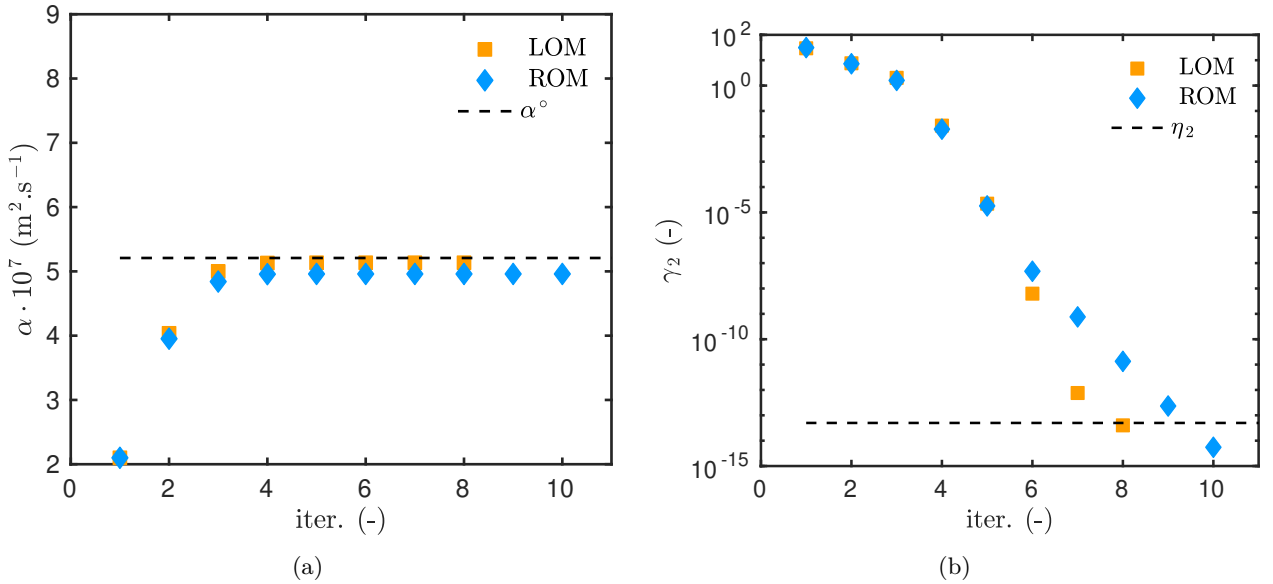


Figure 5. Evolution of the estimated parameter (a) and of the convergence criteria γ_2 according to the iteration.

7 Solving the parameter estimation problem for a real case study

Now the methodology illustrated in Figure 1 is applied to a realistic case study presented in the next section. Then, the reduced sequence of three days is determined using the OED methodology.

7.1 Description of the case study

The studied building is an old house, built at the end of the XIXth century and located in Saint Julien de Crempse, France. Further information on the architectural aspect of the building can be found in [32].

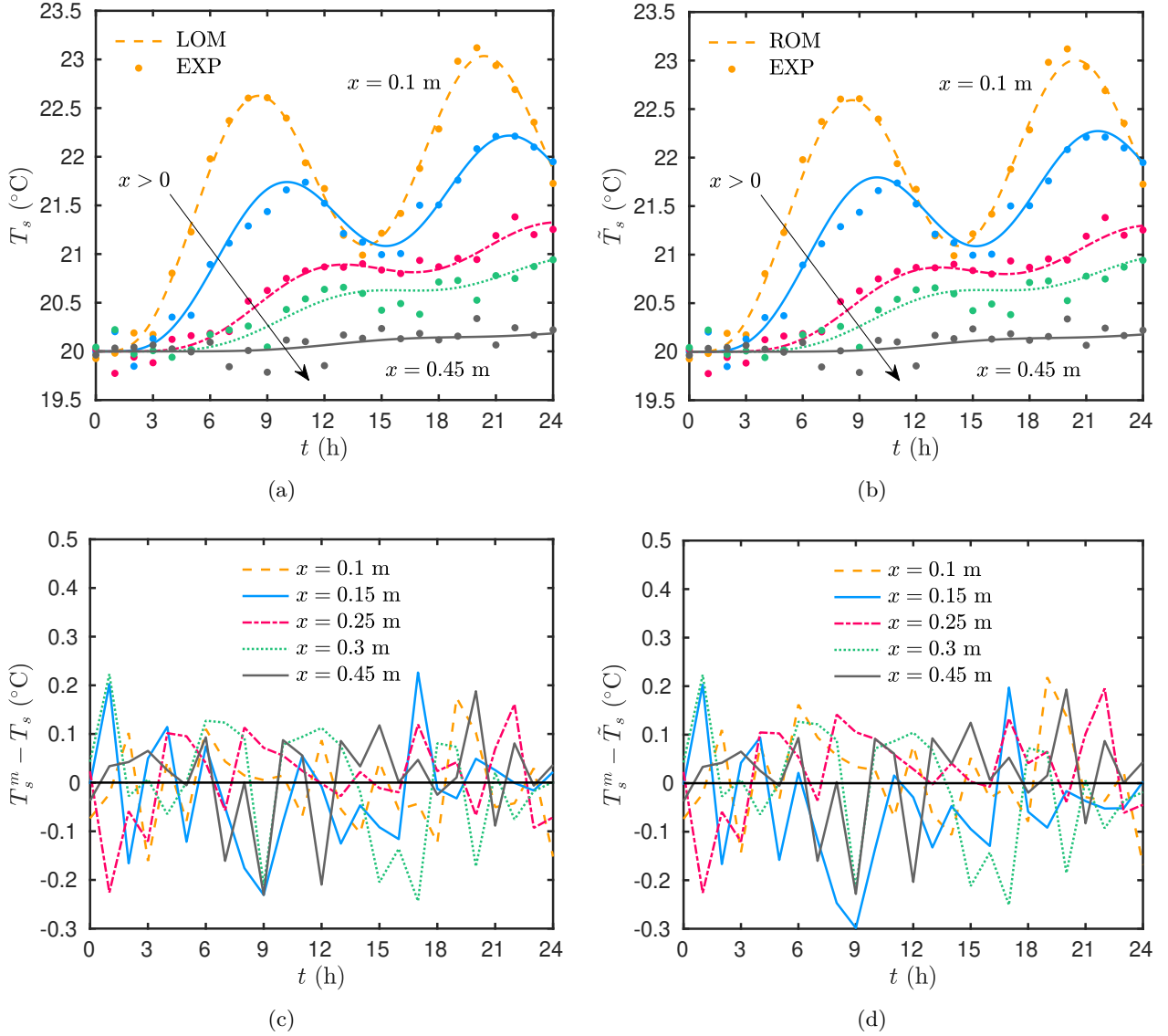


Figure 6. Comparison of the (simulated) measurement and the model prediction using the estimated parameter for the LOM (a,c) and the MIM ROM Order 5 (b,d).

The investigated wall is oriented East and has a length of $L = 43$ cm. The wall is composed of a mixture of lime stones and clay mortar as shown in the picture Figure 8(c). Due to the vernacular traditional architecture, the stones arise from local around the house. There is no information on the exact position of the stones. The issue is to estimate the global thermal diffusivity α of the wall by assuming an equivalent homogenous model [14]. Note that the structural identifiability of this parameter has been demonstrated in [13]. For this aim, the wall are monitored using five intrusive calibrated sensors HOBO TMC-6-HA as shown in Figures 8(a) to 8(c). Three sensors are installed inside the wall by obliquely drilling a whole of 13 mm. In the hole, the contact between the material and the sensor is ensured by a thermal conductive paste. The hole is then filled using an insulation material. The sensor located at the inside and outside surfaces are protected by insulation materials from incident radiation. The location of the sensor is set to assume that the heat transfer occurs mainly from the outside to the inside. An illustration of the experimental design is given in Figure 8(d).

The monitoring is carried out from January until April 2009. Experimental measures of temperature are available at $x = \{5, 23, 40\}$ cm, as illustrated in Figure 9(b). Thus, $N_s = 3$ are hold. It is not known if the sensors are located in the stone or in the mortar. The temperature $T_{\infty,L}$ and $T_{\infty,R}$ are also measured

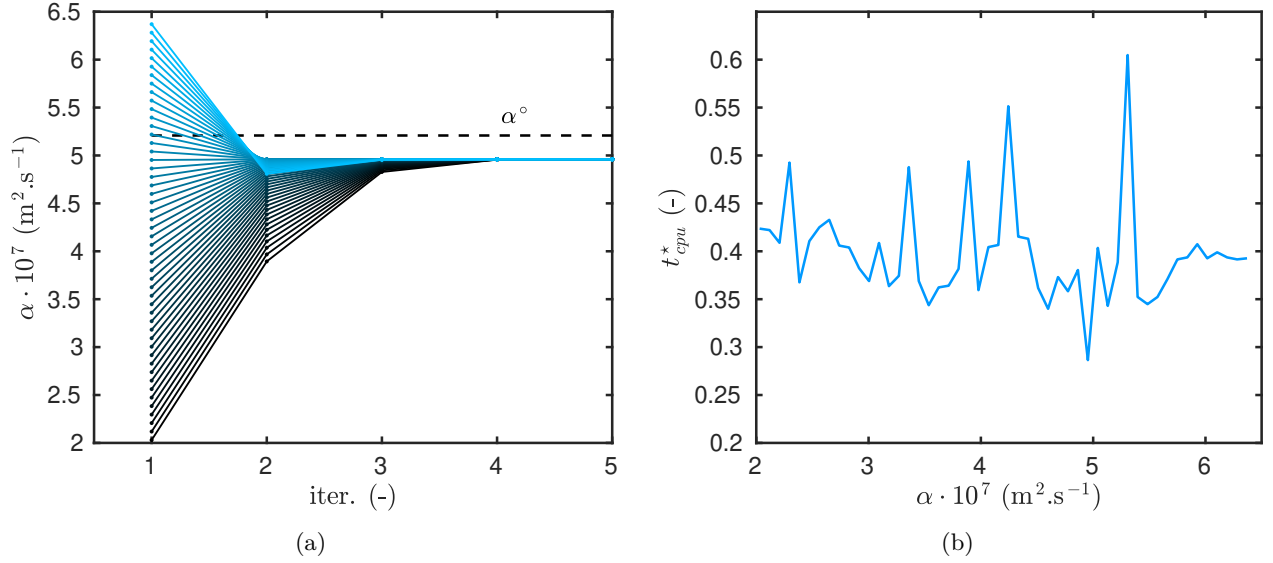


Figure 7. Evolution of the estimated parameter according to the iteration (a) and of the computational time ratio of the algorithm using the MIM ROM Order 5 (b) for 50 values of initial diffusivity.

Table 3. Wall stratigraphy.

Layer	Thermal diffusivity $[\text{m}^{-2} \cdot \text{s}^{-1}]$	Thickness $[\text{cm}]$
Lime stones	$2.7 \cdot 10^{-7}$	$\mathcal{O}(20)$
Mortar	$5.5 \cdot 10^{-7}$	$\mathcal{O}(4)$
Equivalent homogeneous wall	$2.8 \cdot 10^{-7}$	43

and given in Figure 9(a). Measures are available for $\Omega_t = [0, 2670] \text{ h}$, corresponding to four months. The measurement time step is 1 h. The experimental uncertainties σ is computed using [33]:

$$\sigma = \sqrt{\sigma_m^2 + \sigma_x^2},$$

where $\sigma_m = 0.1 \text{ }^\circ\text{C}$ is the sensor measurement uncertainty and σ_x is the sensor position uncertainty. Due to experimental design based on drilling a large wall, the latter can be important. It is computed according to:

$$\sigma_x = \left. \frac{\partial T}{\partial x} \right|_{x=x_s} \delta_x,$$

where $\delta_x = 2 \text{ cm}$ is the uncertainty on the sensor position. The partial derivative $\frac{\partial T}{\partial x}$ is computed using the numerical model. Figure 10(a) shows the probability of the measurement uncertainty at the three points of observation. The uncertainty increases for the sensor located near the outside air conditions. For the initial conditions, a first order polynomial is fitted using the experiment:

$$T_{\text{ini}} : x \mapsto T_0 \cdot \left(1 + \frac{x}{\ell_1} \right),$$

where $T_0 = 11.75 \text{ }^\circ\text{C}$ and $\ell_1 = -0.406 \text{ m}$. As shown in Figure 10(b), the error fitting is satisfactory with $\varepsilon_2 = 0.09 \text{ }^\circ\text{C}^2$. The *a priori* knowledge from standards gives $\alpha^{\text{apr}} = 2.8 \cdot 10^{-7} \text{ m}^2\text{.s}^{-1}$. In addition, Table 3 gives the diffusivity of the different elements composing the wall.



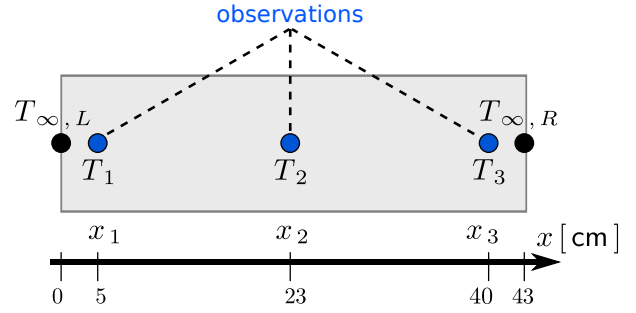
(a)



(b)



(c)



(d)

Figure 8. *Illustration of the experimental design with picture of the inside sensors (a,b), the outside sensors (c) and the experimental design (d).*

7.2 Determining the reduced sequence of observations using the OED methodology

The OED methodology is now carried out to determine the optimal reduced sequence of three days Ω_t^{oed} of observations. The sensitivity function at the point of observations $x_s, s \in \{1, 2, 3\}$ are computed and shown in Figure 11(a). Then, the criteria Ψ is evaluated for each sequence of three days in Ω_t . Figure 11(b) shows the variation of the dimensionless criteria according to the choice of t_{ini} . By comparing Figure 11(a) and 11(b), it can be remarked that the optimal sequences occurs when the sensitivity of the parameter have high magnitudes of variations. The criteria verifies $\Psi \geq 0.98$ for three initial days. According to these results, the following reduced sequence is adopted for the construction of the MIM ROM and then the estimation of the unknown parameters:

$$\Omega_t^{\text{oed}} = [72, 75] \text{ d.}$$

The chosen monitoring time of 3 days arises from a compromise among several opposite criteria. Indeed, it could be reduced compared to traditional methods. From an pure inverse problem point of view, the longest is the measurement period, the highest is the accuracy of the parameter estimation. This can be proven by looking at the variation of the OED criteria Ψ according to the length of the sequence in Figure 12. The criteria is monotonously increasing according to Ω_t^{oed} . However, one has to deal with experimental constraints such as the acceptance of the building occupants. Furthermore, the longer is the measurement

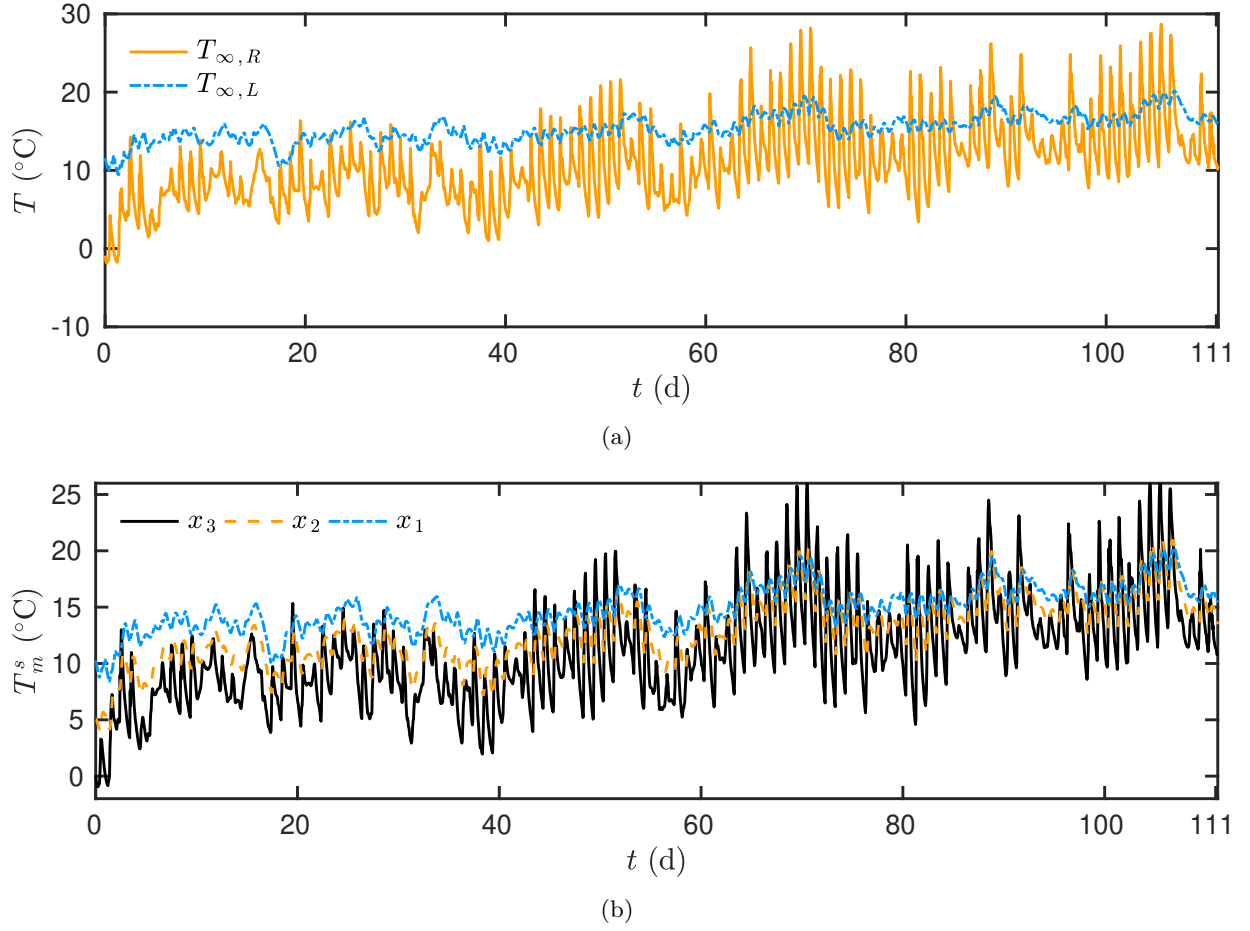


Figure 9. Time variations of the boundary conditions (a) and the measured observation data (b). For the sake of clarity, the measurement uncertainty is not presented.

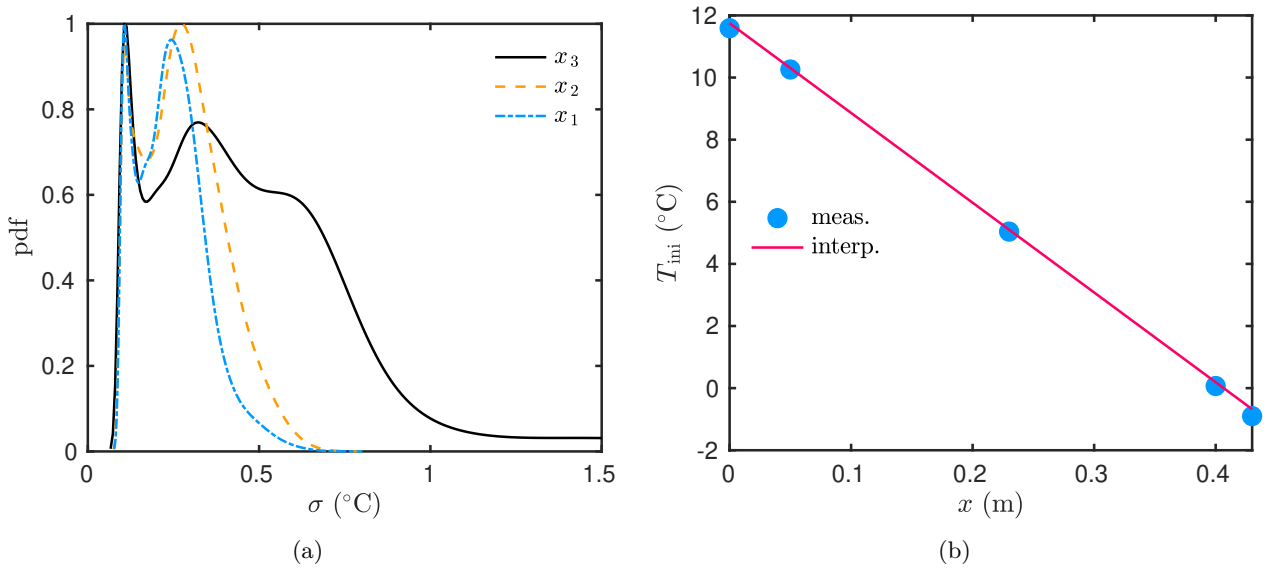


Figure 10. Probability density function of the uncertainty measurement of the observations (a) and initial condition of the problem (b).

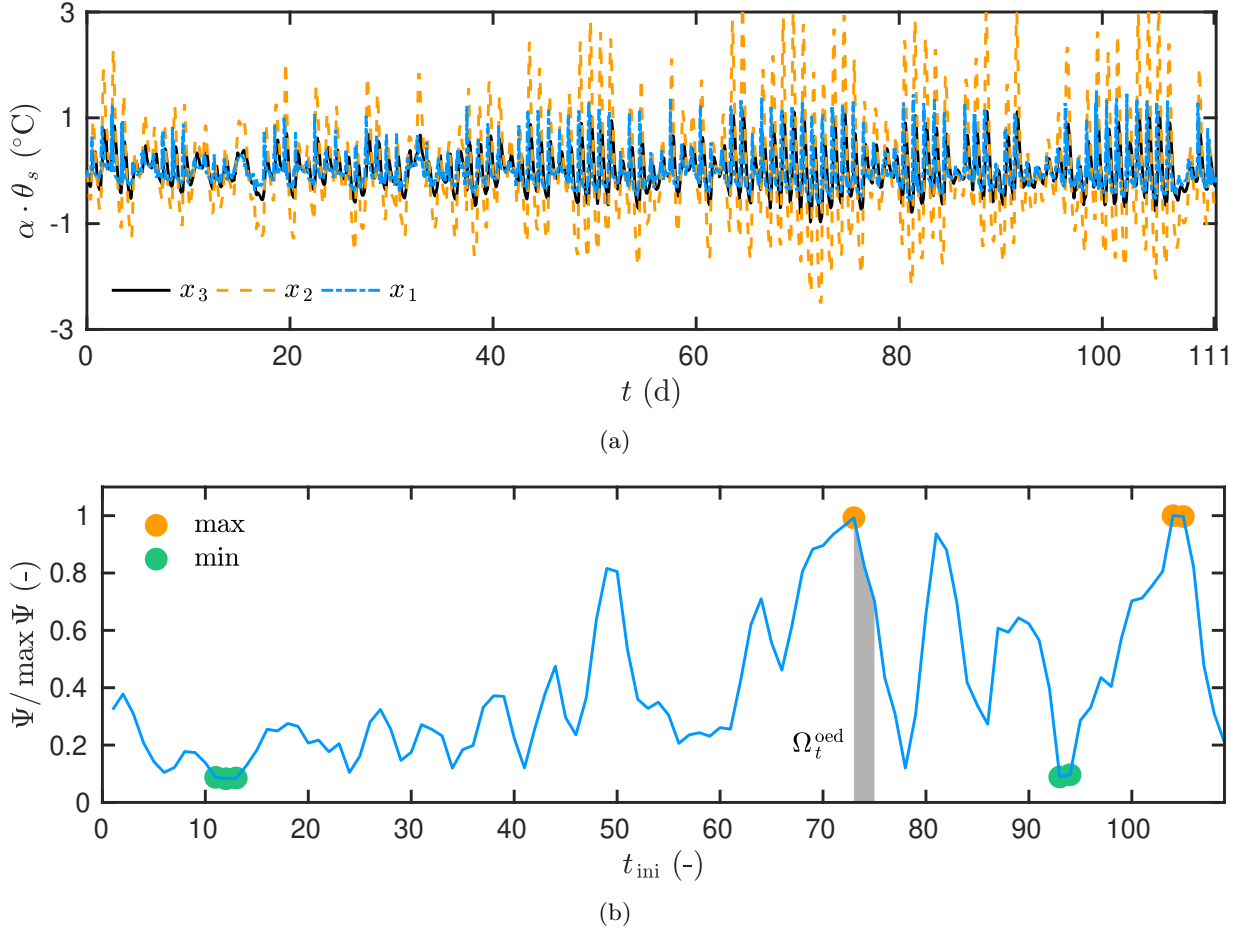


Figure 11. Time variations of the sensitivity functions of the problem (a) and variation of the OED criteria according to the choice of the initial time of the reduced sequence Ω_t^{oed} (b).

period, the higher is the computational time of the direct model and as a consequence the inverse problem algorithm. Figure 12 shows the variation the criteria Ψ added to the inverse of the computational cost of the algorithm. For this case, a good compromise is in three days of monitoring. Note that the influence of the length of the measurement period is investigated empirically in [12]. For their case study, the authors suggest to carry at least three days of monitoring to have an accurate estimation.

7.3 Building the MIM ROM

For the reduced sequence Ω_t^{oed} , the boundary conditions are given in Figure 13(a). The initial condition is the following:

$$T_{\text{ini}} : x \mapsto T_0 \cdot \left(1 + \frac{x}{\ell_1} - \left(\frac{x}{\ell_2} \right)^2 \right),$$

where $T_0 = 16.87$ °C, $\ell_1 = 1.764$ m and $\ell_2 = 0.5$ m. The error fitting of the initial condition is satisfactory ($\varepsilon_2 = 0.24$ °C²) as shown in Figure 13(b). The learning step is carrying considering four values of diffusivity $\Omega_\alpha = \{1, 5, 10, 70\} \cdot 10^{-7} \text{ m}^2 \cdot \text{s}^{-1}$. The training is carried until the order $N = 20$ taking around $t_{\text{cpu}} = 3$ d. Figures 14(a) and 14(b) shows the evolution of the error according to the order of the model. It can be remarked that a model of order $N = 10$ provides a satisfactory accuracy.

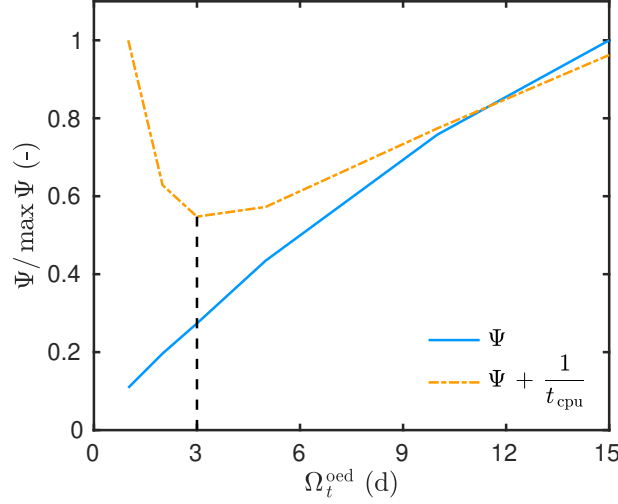


Figure 12. Variation of the OED criteria according to the length of the reduced sequence Ω_t^{OED} and the computational time of the MIM ROM.

Table 4. Results of the parameter estimation problem, noting that $\alpha^{\text{apr}} = 2.8 \cdot 10^{-6} \text{ m}^2 \cdot \text{s}^{-1}$.

Model	Order	Estimated parameter		Computational time		Iterations to to converged
		$\alpha^\circ \cdot 10^7 [\text{m}^2 \cdot \text{s}^{-1}]$		$t_{\text{cpu}} [\text{s}]$	$t_{\text{cpu}}^* [-]$	
LOM	100	1.064		572	1	19
ROM	5	1.097		114	0.2	24
ROM	7	1.064		112	0.19	23
ROM	10	1.062		101	0.17	21
ROM	15	1.065		102	0.18	21
ROM	20	1.067		94	0.16	19

7.4 Parameter estimation

After the learning step the MIM ROM matrices are known. Thus, the model is now used to estimate the thermal diffusivity of the material. Figure 13(d) shows the variation of the sensitivity functions using the *a priori* value of the diffusivity. The functions have high magnitude of variations ensuring the practical identifiability of the unknown parameter. The GAUß algorithm can be employed for the parameter estimation. It uses the MIM ROM of order $N = 10$ over the reduced sequence Ω_t^{OED} . The observations are shown in Figures 13(c). Figure 15(a) shows the evolution of the estimated parameter. The algorithm requires 24 iterations to satisfy the convergence criteria, which evolution is illustrated in Figure 15(b). In approximately 10 iterations, the algorithm already finds a trusting value of the thermal diffusivity. Note that the stability of the estimation have been verified by providing several values of initial guess in the algorithm. As presented in Table 4, the value of the estimated parameter α° remains stable from $N = 7$. The computational time to solve the inverse problem is cut by 5 compared to the LOM. Slightly differences in the computational time are remarked for the MIM ROM due to the number of iterations to converge. The model of order 20 is more accurate and requires less iterations to retrieve the unknown parameter. It is important to note that the experimental design relies on embedded sensors inside the wall to obtain the experimental observations. This may be a restriction of the methodology for other case study. Other experimental devices could be used such as heat flux sensor or infrared camera. The methodology to search the optimal experimental design could be extended for such approaches. Furthermore, a MIM ROM needs to be constructed according to the new type of observable field.

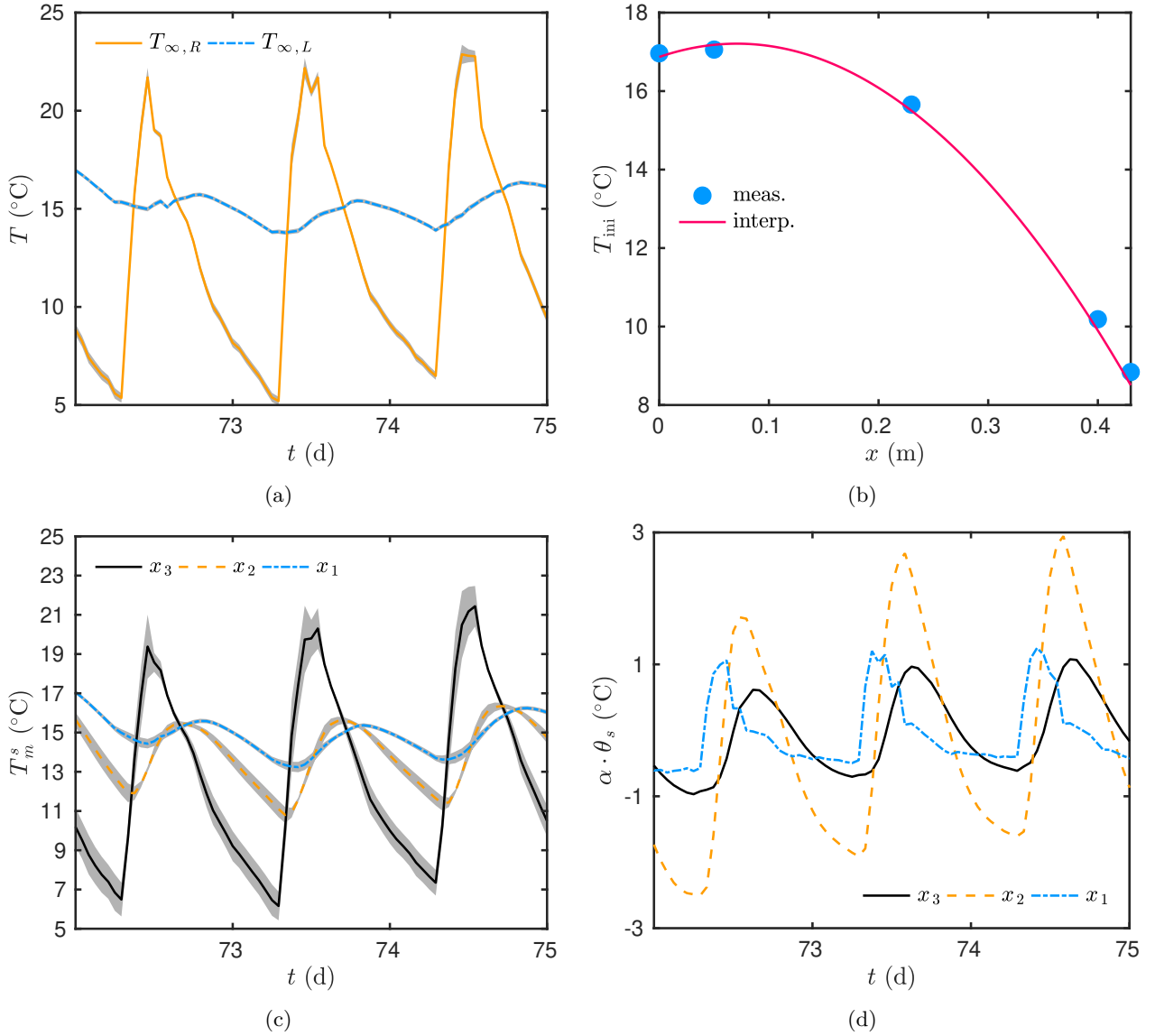


Figure 13. Time variations of the boundary conditions (a) and and initial condition of the problem (b) for the reduced sequence Ω_t^{red} . Time variation of the measured observation data (c) and the sensitivity functions (d). The grey shadow corresponds to the measurement uncertainty.

7.5 Reliability of the model

To evaluate the reliability of the model with the estimated thermal diffusivity $\alpha^\circ = 1.06 \cdot 10^{-6} \text{ m}^2 \cdot \text{s}^{-1}$, the numerical predictions computed with the MIM ROM $N = 10$ are compared to the experimental observations at each point x_s , for the whole sequence Ω_t . Figures 16(a),16(c) and 16(e) show this juxtaposition for the last week of the measurement. The model using *a priori* parameter lacks of accuracy to represent the physical phenomena. The model with the estimated parameter has a better reliability. However, for the point x_3 , both models faces some discrepancy with the experimental observations. It can be noted a certain delay between the prediction and the observation at the point x_2 . Figures 16(b),16(d) and 16(f) give the probability of the error with observation over the whole sequence of measurement. The error is compared with the probability of the measurement. The prediction of the model are more precised using the estimated parameter. Indeed the probability has a smaller standard deviation. However, at the point x_3 , errors of larger magnitude occur for probabilities of both models. It reveals that some phenomena are not considered in the model and the mathematical formulation should be improved by considering for instance

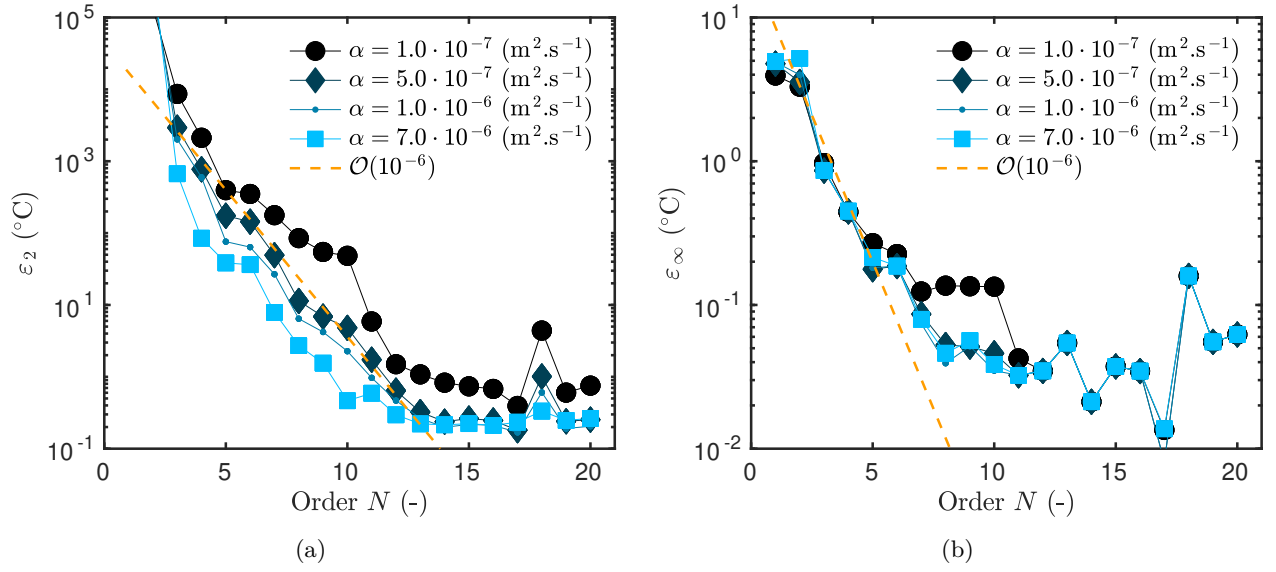


Figure 14. Evolution of the error of the MIM ROM model according to the order N trained over the reduced sequence Ω_t^{red} .

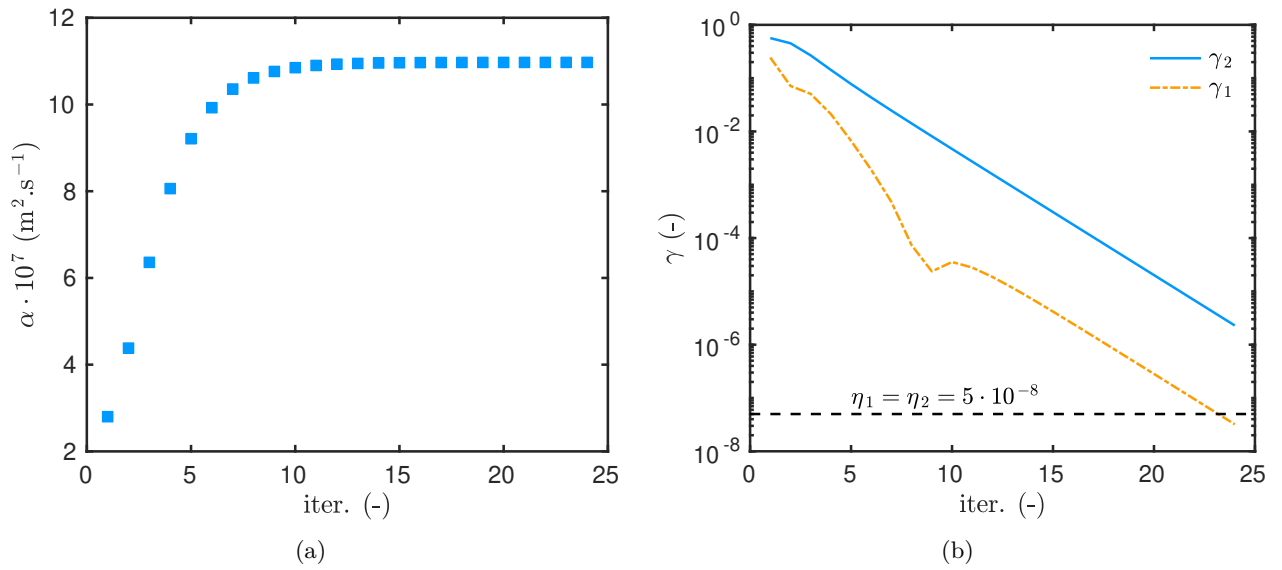


Figure 15. Evolution of the estimated parameter α (a) and of the convergence criteria (b) according to the iteration number of the algorithm.

heterogeneous diffusivity in the wall. To verify the reliability of the proposed model, the inside heat flux j and the thermal loads E are computed according to:

$$j \stackrel{\text{def}}{=} -k \left. \frac{\partial T}{\partial x} \right|_{x=L}, \quad E \stackrel{\text{def}}{=} \int_{\Omega_t} j_q \, d\tau.$$

Figure 17(a) shows the variation of the thermal flux. It has important magnitude inducing high thermal loads as noted in Figure 17(b). The thermal loads are computed for perturbations of 20% of the estimated diffusivity. It can be noted that the relative error on the loads remains stable around 5%. It confirms that the approximations introduced from the whole methodology (uncertainty measurement, reduced order model or estimation on a reduced sequence) are minor compared to the ones in the mathematical model itself.

8 Conclusion

The uncertain thermal properties of existing building walls can be determined by solving parameter estimation problems. However, such problems have important computational cost for at least two reasons. The inverse problem algorithm requires to solve the direct problem several times. In addition, the experimental measurement are carried on-site implying simulations over several month under climatic variations. These complexities increase the computational requirements.

To answer this issue, an innovative methodology is proposed based on two concepts. First, a reduced order model based on MIM method is used to reduce significantly the computational time of the direct problem without loosing accuracy. The methodology is presented in Section 3. The reduced model is based on a state space representation where the matrices are built during a learning step. The latter is based on a minimization procedure between the predictions of the reduced and complete models. An interesting point is that the model is built to compute the field of interest and its sensitivity to the unknown parameter. The sensitivity is known straightforwardly using the matrices of the reduced model.

The second concept is the optimal experiment design methodology, described in Section 4. It is employed to determine a reduced sequence of observations. Three advantages are enhanced with this approach. First, it reduces the inherent computational cost of a *a posteriori* model reduction methods since the learning step is carried for a reduced sequence. Then, the chosen sequence is optimal to estimate the parameter with accuracy. In addition, the inverse problem is solved only for a few days of observations. It reduced again the computational effort to retrieve the parameter. The solution of the inverse problem is obtained with the GAUß algorithm since the reduced order model computes the field and its sensitivity.

A first case study is proposed in Section 6 to validate the MIM model reduction method. This step is important to evaluate the efficiency in terms of accuracy and computational cuts. The MIM model is built with a signal based on 4 values of thermal diffusivity. Then, the MIM model shows a very satisfying accuracy to simulate the direct problem over a wide range of diffusivity. Regardless the inherent cost of the learning step, the model cut by 5 the computational cost of the direct problem. The model is also evaluated in the framework of inverse problem with simulated experimental observations. The unknown parameter is estimated with an error lower than the measurement uncertainty and a reduced computational time.

After this simple validation case, the whole methodology is applied to a more realistic one. The issue is to estimate the thermal diffusivity of an old building wall. The latter is monitored during four months with three sensors drilled inside. With the OED methodology, a sequence of three days is identified as optimal. Then, the MIM ROM is built for the reduced sequence and a signal composed of 4 values of thermal diffusivity. Then, a model of order 10 is chosen to solve the inverse problem. The estimated diffusivity is three times higher than the one provided by standards. In terms of computational efficiency, the parameter is estimated with an algorithm 5 times faster. Eventually, the reliability of the model is evaluated by comparing the predictions of the MIM model with the experimental observations of the complete period. It highlights that the global methodology is efficient to calibrate the model with a reduced computational effort.

Future works should focus on improving the definition of the mathematical model by dealing with anisotropic thermal diffusivity in the building wall. In addition, to evaluate the real efficiency of the methodology, the GAUß algorithm combined with the MIM ROM should be installed in embedded system for fast estimation of building material properties.

Acknowledgments

BK thanks Johnathan Gerardin for the fruitful discussions on MIM.

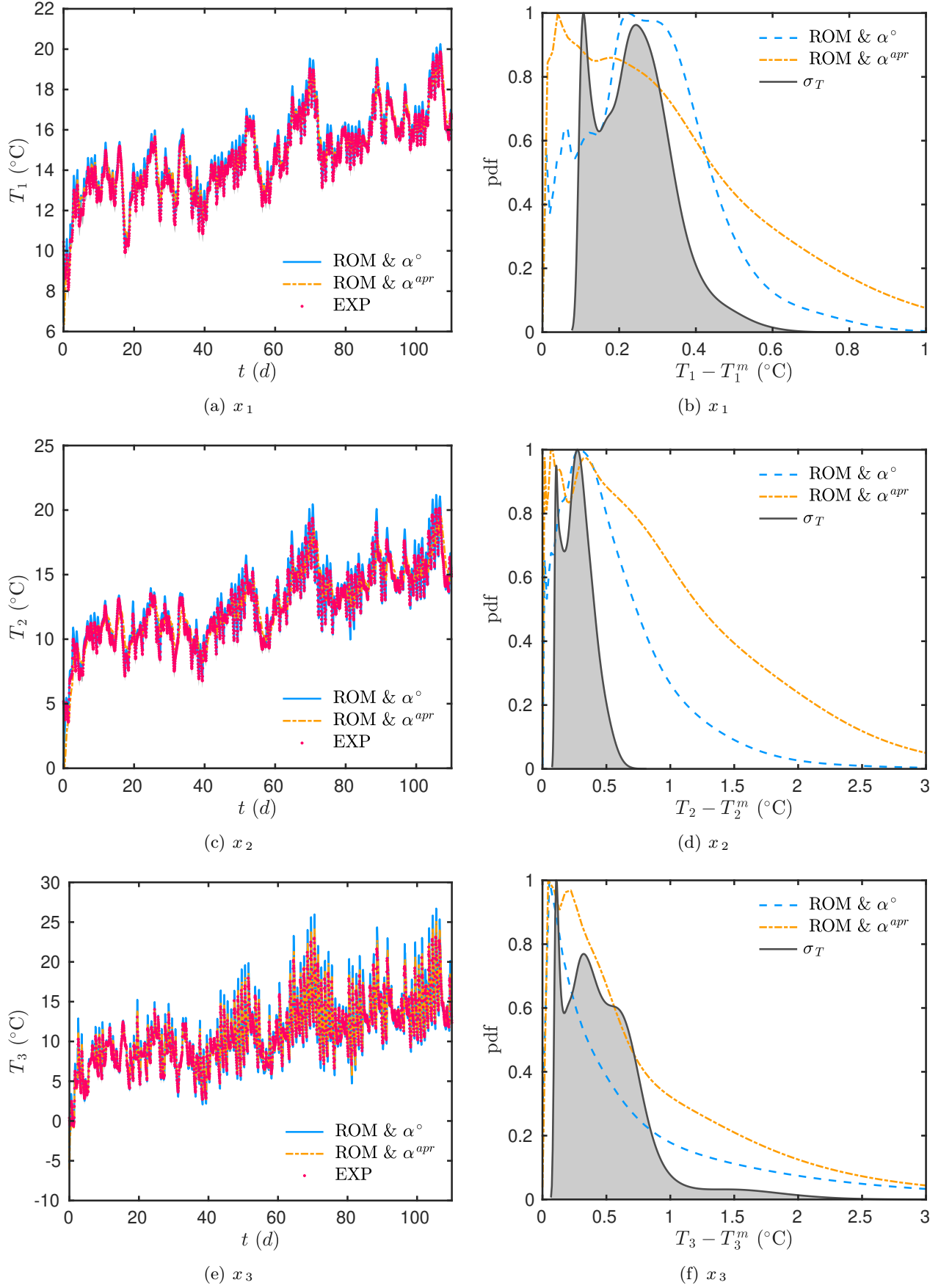


Figure 16. Comparison of the numerical predictions for the last week (a,c,e) and probability of the error between the predictions and the experimental observations for the whole period Ω_t (b,d,f).

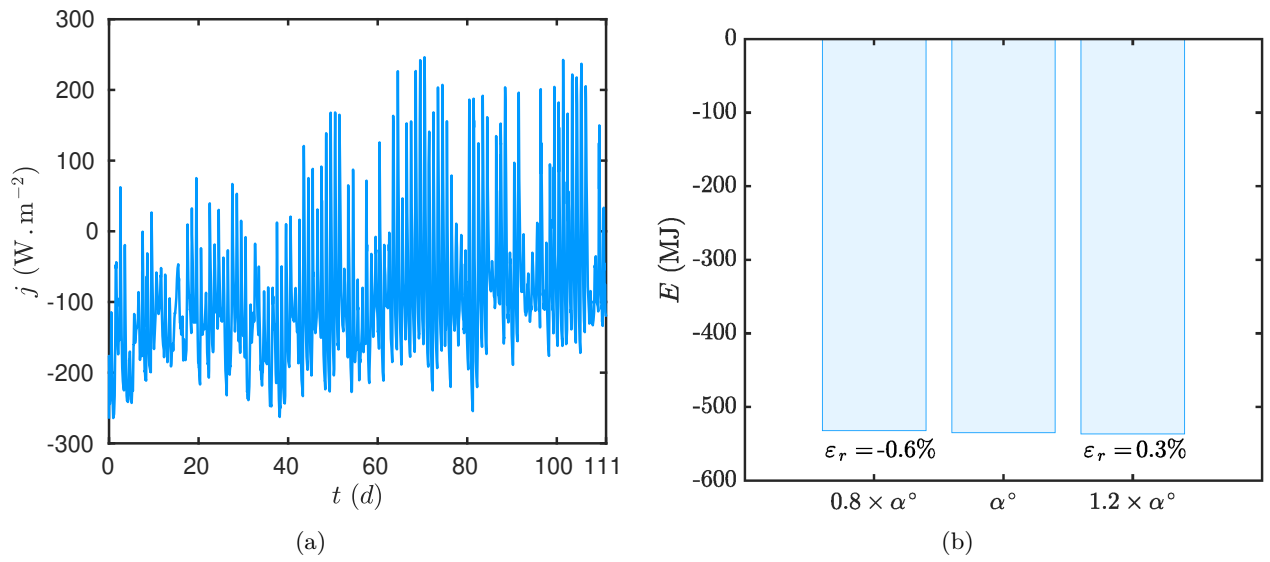


Figure 17. Time evolution of the inside heat flux (a) and variation of the thermal loads according to small perturbation of α° (b).

Nomenclature and symbols

<i>Physical parameters</i>		
Latin letters		
c	volumetric heat capacity	$[\text{J} \cdot \text{m}^{-3} \cdot \text{K}^{-1}]$
E	thermal loads	$[\text{J}]$
j	heat flux	$[\text{W} \cdot \text{m}^{-2}]$
k	thermal conductivity	$[\text{W} \cdot \text{m}^{-1} \cdot \text{K}^{-1}]$
L	length	$[\text{m}]$
t	time	$[\text{s}]$
x	position	$[\text{m}]$
T	temperature	$[\text{K}]$
Greek letters		
α	thermal diffusivity	$[\text{m}^2 \cdot \text{s}^{-1}]$
δ	sensor position uncertainty	$[\text{m}]$
σ	measurement uncertainty	$[\text{K}]$
Ω_α	thermal diffusivity interval	$[\text{m}^2 \cdot \text{s}^{-1}]$
Ω_t	time interval	$[\text{s}]$
Ω_t^{oad}	optimal time interval	$[\text{s}]$
$\varepsilon, \varepsilon_2$	error	$[\text{K}]$
ε_r	relative error	$[-]$

<i>Mathematical notations</i>	
Latin letters	
$A, B, C, F, G,$ H, Q, U, X, Y	matrices
\mathcal{F}	FISHER matrix
F_o	FOURIER number
J	cost function
p	unknown parameter
u	dimensionless temperature
N_r	order of the reduced model
N_s	number of sensors
Greek letters	
Δx	space mesh
Δt	time step
η_1, η_2	tolerance value
γ_1, γ_2	convergence criteria
Π	measurement plan
Ψ	D-optimum criteria
θ	dimensionless sensitivity
$\varepsilon, \varepsilon_2, \varepsilon_r$	error
Subscripts and superscripts	
apr	<i>a priori</i> parameter
cpu	computational cost
f	final
ini	initial
m	measurement
min	minimal value
ref	reference value
rom	reduced order model
r	real value
s	sensor
x	position
\circ	estimated parameter
\star	dimensionless value
∞	boundary

References

- [1] E. Stephan, R. Cantin, A. Caucheteux, S. Tasca-Guernouti, and P. Michel. Experimental assessment of thermal inertia in insulated and non-insulated old limestone buildings. *Building and Environment*, 80:241–248, 2014. [1](#)
- [2] C. Cornaro, V. Adoo Puggioni, and R. Maria Strollo. Dynamic simulation and on-site measurements for energy retrofit of complex historic buildings: Villa mondragone case study. *Journal of Building Engineering*, 6:17–28, 2016. [1](#)

- [3] L. Evangelisti, C. Guattari, P. Gori, and R. Vollaro. In situ thermal transmittance measurements for investigating differences between wall models and actual building performance. *Sustainability*, 7(8):10388–10398, 2015. [1](#)
- [4] E. Hamard, B. Lemerrier, B. Cazaciu, A. Razakamanantsoa, and J.C. Morel. A new methodology to identify and quantify material resource at a large scale for earth construction – application to cob in brittany. *Construction and Building Materials*, 170:485–497, 2018. [1](#)
- [5] L. Evangelisti, C. Guattari, P. Gori, and F. Asdrubali. Assessment of equivalent thermal properties of multilayer building walls coupling simulations and experimental measurements. *Building and Environment*, 127:77–85, 2018. [1](#), [2](#)
- [6] A. Jumabekova, J. Berger, and A. Fouquier. Sensitivity analysis in the framework of parameter estimation problem for building energy performance: a continuous derivative based approach. *submitted*, pages 1–31, 2019. [1](#)
- [7] T. Busser, M. Pailha, A. Piot, and M. Woloszyn. Simultaneous hygrothermal performance assessment of an air volume and surrounding highly hygroscopic walls. *Building and Environment*, 148:677 – 688, 2019. [1](#)
- [8] J. Berger, H.R.B. Orlande, N. Mendes, and S. Guernouti. Bayesian inference for estimating thermal properties of a historic building wall. *Building and Environment*, 106(Supplement C):327–339, 2016. [1](#)
- [9] A. Rasooli and L. Itard. In-situ rapid determination of walls’ thermal conductivity, volumetric heat capacity, and thermal resistance, using response factors. *Applied Energy*, 253:113539, 2019. [1](#), [2](#)
- [10] A. Rasooli and L. Itard. In-situ characterization of walls’ thermal resistance: An extension to the iso 9869 standard method. *Energy and Buildings*, 179:374 – 383, 2018. [2](#)
- [11] T. Suklje, M. Hamdy, C. Arkar, J.L.M. Hensen, and S. Medved. An inverse modeling approach for the thermal response modeling of green façades. *Applied Energy*, 235:1447–1456, 2019. [2](#)
- [12] A. Rodler, S. Guernouti, and M. Musy. Bayesian inference method for in situ thermal conductivity and heat capacity identification: Comparison to iso standard. *Construction and Building Materials*, 196:574–593, 2019. [2](#), [18](#)
- [13] J. Berger and D. Dutykh. Evaluation of the reliability of building energy performance models for parameter estimation. *Computational technologies*, 4(3):1–13, 2019. [2](#), [14](#)
- [14] P. Gori, L. Evangelisti, and C. Guattari. Description of multilayer walls by means of equivalent homogeneous models. *International Communications in Heat and Mass Transfer*, 91:30–39, 2018. [2](#), [14](#)
- [15] N. Simoes, I. Simoes, A. Tadeu, C.A.B. Vasconcellos, and W.J. Mansur. 3d transient heat conduction in multilayer systems – experimental validation of semi-analytical solution. *International Journal of Thermal Sciences*, 57:192–203, 2012. [2](#)
- [16] D. Ucinski. *Optimal Measurement Methods for Distributed Parameter System Identification*. CRC Press, New York, 2004. [2](#), [7](#)
- [17] J. V. Beck and K. J. Arnold. *Parameter Estimation in Engineering and Science*. John Wiley and Sons, New York, 1977. [2](#), [7](#)
- [18] J. Berger, D. Dutykh, and N. Mendes. On the optimal experiment design for heat and moisture parameter estimation. *Experimental Thermal and Fluid Science*, 81:109 – 122, 2017. [2](#)
- [19] J. Berger, T. Busser, D. Dutykh, and N. Mendes. An efficient method to estimate sorption isotherm curve coefficients. *Inverse Problems in Science and Engineering*, 0(0):1–38, 2018. [2](#), [7](#)

- [20] G. D'Alessandro and F. de Monte. Optimal experiment design for thermal property estimation using a boundary condition of the fourth kind with a time-limited heating period. *International Journal of Heat and Mass Transfer*, 134:1268–1282, 2019. 2
- [21] J. Berger, N. Mendes, S. Guernouti, M. Woloszyn, and F. Chinesta. Review of Reduced Order Models for Heat and Moisture Transfer in Building Physics with Emphasis in PGD Approaches. *Archives of Computational Methods in Engineering*, pages 1–13, jul 2016. 2
- [22] D. Petit, R. Hachette, and D. Veyret. A Modal Identification Method To Reduce A High-Order Model: Application To Heat Conduction Modelling. *International Journal of Simulation Modelling*, 17(4):242–250, 1997. 2
- [23] M. Girault, D. Petit, and E. Videcoq. The Use of Model Reduction and Function Decomposition for Identifying Boundary Conditions of A Linear Thermal System. *Inverse Problems in Engineering*, 11(5):425–455, 2003. 2
- [24] M. Girault and D. Petit. Resolution of linear inverse forced convection problems using model reduction by the Modal Identification Method: application to turbulent flow in parallel-plate duct. *International Journal of Heat and Mass Transfer*, 47(17-18):3909–3925, 2004. 2
- [25] M. Girault and D. Petit. Identification methods in nonlinear heat conduction. Part I: Model reduction. *International Journal of Heat and Mass Transfer*, 48(1):105–118, 2005.
- [26] M. Girault and D. Petit. Identification methods in nonlinear heat conduction. part ii: inverse problem using a reduced model. *International Journal of Heat and Mass Transfer*, 48(1):119 – 133, 2005. 2
- [27] J. Gérardin, M.H. Aumeunier, M. Firdaouss, J.L. Gardarein, and F. Rigollet. Réduction de modèle thermique par Méthode d'Identification Modale (MIM) pour déterminer la température de surface des composants de machine de fusion. In *Congrès Français de Thermique 2017*, volume 1 of *Actes du Congrès Français de Thermique 2017*, ISBN : 978-2-905267-92-4, pages 567–574. IUSTI & les laboratoires de la fédération Fabri de Peiresec, Aix-Marseille Université, 2017. 2
- [28] M. Necati Ozisik and H. R.B. Orlande. *Inverse Heat Transfer: Fundamentals and Applications*. CRC Press, New York, 2000. 3, 7
- [29] A. Nayfeh. *Perturbation Methods*. Wiley VCH, New York, 2000. 3
- [30] W. Kahan and J. Palmer. On a proposed floating-point standard. *ACM SIGNUM Newsletter*, 14:13–21, 1979. 3
- [31] A. Jumabekova, J. Berger, A. Fouquier, and G.S. Dulikravich. Searching an optimal experiment observation sequence to estimate the thermal properties of a multilayer wall under real climate conditions. submitted, pages 1–28, 2020. 7
- [32] R. Cantin, J. Burgholzer, G. Guarracino, B. Moujalled, S. Tamelikecht, and B.G. Royet. Field assessment of thermal behaviour of historical dwellings in france. *Building and Environment*, 45(2):473 – 484, 2010. 13
- [33] P. J. Taylor. The stability of the Dufort-Frankel method for the diffusion equation with boundary conditions involving space derivatives. *The Computer Journal*, 13(1):1–92, 1970. 15